Energy structure of Eu^{3+} centres in CdF_2–CaF_2:Eu superlattices on silicon

2007 J. Phys.: Condens. Matter 19 395023

(http://iopscience.iop.org/0953-8984/19/39/395023)

J. Phys.: Condens. Matter **19** (2007) 395023 (9pp) doi:10.1088/0953-8984/19/39/395023

Energy structure of Eu^{3+} centres in CdF_2–CaF_2:Eu superlattices on silicon

V A Chernyshev[1], A V Abrosimov[1], S V Gastev[2], A V Krupin[2], A E Nikiforov[1], J K Choi[3], R J Reeves[3], S M Suturin[2] and N S Sokolov[2]

[1] Ural State University, 51 Lenin Avenue, Ekaterinburg 620083, Russia
[2] A F Ioffe Physico-Technical Institute, 26 Polytechnicheskaya, St Petersburg 194021, Russia
[3] University of Canterbury, Rutherford Boulevard, Christchurch PB4800, New Zealand

E-mail: vladimir.chernyshev@usu.ru

Received 28 February 2007, in final form 1 May 2007
Published 30 August 2007
Online at stacks.iop.org/JPhysCM/19/395023

Abstract

Stark energy levels of Eu^{3+} ($4f^6$) ions in CdF_2–CaF_2:Eu epitaxial superlattices on Si have been measured by laser spectroscopy and calculated in an exchange charge model. Two types of centre have been considered in the CaF_2 layer: an 'interface centre', close to the CdF_2/CaF_2 interface, and a 'remote centre' located in the core of a layer. The influence of distortion, created by the silicon substrate, has been taken into consideration. The calculations confirmed a previously suggested 'electron' model of the interface centre.

1. Introduction

It is known that cubic CaF_2 and CdF_2 crystals are wide band gap materials, $E_g(CaF_2) = 12.1$ eV, $E_g(CdF_2) = 8.0$ eV. Their lattice parameters (5.46 and 5.39 Å respectively) are quite close to that of Si (5.43 Å). This enables growing high structural quality pseudomorphic (coherent with the substrate) superlattices (SLs) on Si(111) [1]. In these SLs strain lowers the crystal symmetry of the fluorite layers from cubic to rhombohedral.

It was revealed that in such SLs with Eu-doped CaF_2 layers ultraviolet photoexcitation is accompanied by efficient tunnelling from excited state of Eu^{2+} ions into the CdF_2 conduction band [2]. This results in conversion of Eu^{2+} into Eu^{3+}, which is most efficient near the CdF_2/CaF_2:Eu interfaces. By means of laser spectroscopy it has been recently found that the positions of the Eu^{3+} energy levels for the interface (I) centre having nine Ca and three Cd cation neighbours and the remote (R) centre with 12 Ca cation neighbours are noticeably different. Taking into account temperature and additional illumination dependences of the interface centre photoluminescence (PL) intensity, it was suggested that in this centre extra electron charge compensation is provided by an electron trapped by a Cd ion neighbouring the Eu^{3+} ion [3, 4].

0953-8984/07/395023+09$30.00

Table 1. Sample description.

Sample number	Thickness of each CaF_2:Eu layer, nm (ML)	Number of periods
1651	3.28 (20)	8
3178	1.90 (7)	20
3172	1.57 (5)	30
3173	0.94 (3)	50
1885	0.63 (2)	75

In this work, we present the results of high-resolution spectroscopic measurements of the $^5D_1$ and $^7F_1$ triplet splitting for the interface and remote centres and compare them with calculations in the exchange charge model [5].

2. Experimental details

All samples were grown at the Ioffe Institute using a conventional molecular beam epitaxy (MBE) process. Layers of CaF_2 and CdF_2 were sequentially deposited on (111)-oriented Si substrates. The opposite signs of the fluoride lattice mismatches with Si allow pseudomorphic growth of the films with the fluoride lattices oriented with (111) plane parallel to the surface. The key specifications of the samples under investigation in this work are summarized in table 1. The thickness of each layer ranged from 2 to 20 monolayers (ML) with symmetric thicknesses of CaF_2 and CdF_2 used in all cases.

Divalent Eu ions were exclusively doped into every CaF_2 layer with a typical concentration of ∼0.1 mol%. The number of superlattice periods was varied inversely with layer thickness so that the total film thicknesses were about the same (see table 1).

The optical measurements were carried out at the University of Canterbury. Combined excitation emission spectroscopy (CEES) was used to study centres of Eu^{3+} in the SLs. A tunable Pyrromethene 546 dye laser pumped by a Spectra-Physics argon laser (2045E) was used to excite Eu^{3+} ions from the ground $^7F_0$ state to the $^5D_1$ state. A 0.3 m focal length spectrometer equipped with a CCD detector was used to monitor the $^5D_0 \rightarrow {}^7F_j$ and $^5D_1 \rightarrow {}^7F_j$ transitions of the Eu^{3+} centres. All samples were mounted on the cold finger of an Oxford Microstat liquid helium cryostat that had a base temperature of ∼4 K. Excitation and emission collection at angles of 50° and 70°, respectively, relative to the normal, were used to reveal the polarization anisotropy in the $^7F_0 \rightarrow {}^5D_1$ and $^5D_0 \rightarrow {}^7F_1$ magneto-dipole optical transitions.

3. Laser spectroscopy of the $^5D_1$ and $^7F_1$ triplet splitting

The [111] C_3 anisotropy axis coinciding with the surface normal vector can be expected in optical properties of Eu^{3+} ions in these SLs because of their coherent growth with Si(111) substrate. Polarization measurements of laser excitation and emission light with $E \parallel [111]$ (π) and $E \perp [111]$ (σ) revealed crystal-field splitting of the strongest $^7F_0 \rightarrow {}^5D_1$ and $^5D_0 \rightarrow {}^7F_1$ magneto-dipole optical transitions for the interface Eu^{3+} centre. Figures 1(a) and (b) show that there are two excitation transitions at 525.33 and 525.26 nm, corresponding to 2.5 cm^{-1} splitting of the $^5D_1$ manifold. The crystal-field splitting of the $^7F_1$ manifold is observed with orthogonal polarization of excitation and emission (figures 1(c) and (d)). Here we see two emission peaks for the I-centre, at 590.06 and 590.57 nm, corresponding to 14 cm^{-1} splitting between the levels.

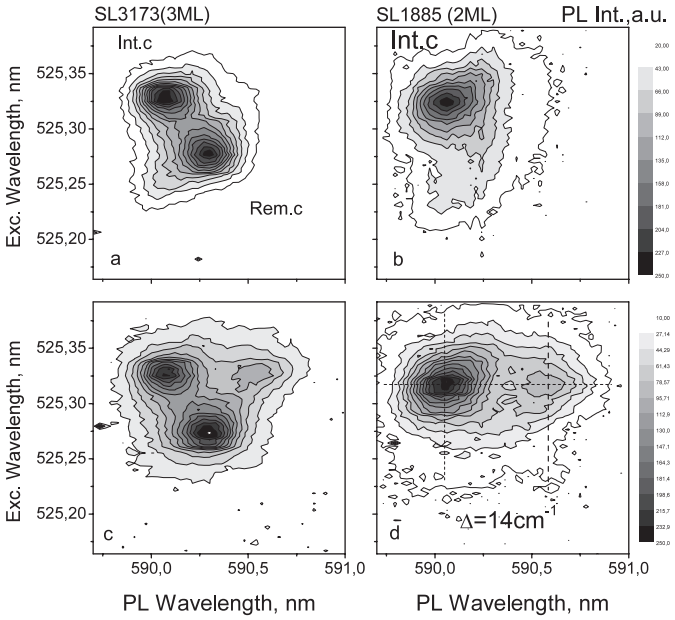

Figure 1. Polarized combined excitation–emission spectra of 3 ML and 2 ML SLs: (a) and (c) with σ-polarized excitation and π-polarized emission; (b) and (d) with π-polarized excitation and σ-polarized emission.

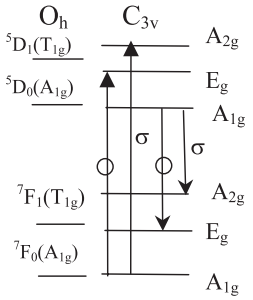

Figure 2. Energy level symmetry and polarization assignments for optical transitions of Eu^{3+} ions in C_{3v}.

Polarization anisotropy measured in these spectra can determine the symmetry assignment of the energy levels. Following Dieke's [6] notation we can assign the relevant transition labels as shown in figure 2 for σ-polarized $A_{1g} \leftrightarrow A_{2g}$ and $A_{1g} \leftrightarrow E_g$ circular polarized transitions in a C_{3v} symmetry centre. It should be noted that we did not observe any splitting for the R-centre in 3, 5 and 7 ML SLs.

It is noteworthy that the transition wavelengths observed here are very close to those measured for the cubic (O_h) centre in CaF_2:Eu bulk crystals [7, 8]. Evidently there is the 0.3% of epitaxial (111) planar strain of the coherent CaF_2 layers at 5 K that should lead to some splitting of the R-centre triplet transitions. The splitting was observed in the 20 ML SL sample where the R-centre photoluminescence is dominant and the I-centre is presented like a weak shoulder. The figure 3(a) shows the strain R-centre splitting of the $^5D_1$ manifold with σ-polarization of excited light and figure 3(b) with its cross-section (figure 3(c)) together

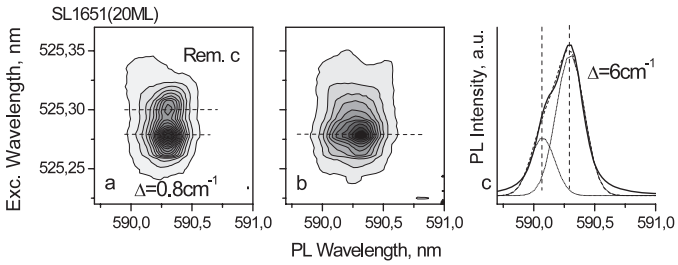

Figure 3. Polarized CEES plots for a 20 ML SL (#1651): (a) with σ-polarized excitation and π-polarized emission and (b) with π-polarized excitation and σ-polarized emission at 5 K. (c) The cross-section of plot (b) with two-peak separation fitting (dotted lines).

demonstrate the same for the $^7F_1$ manifold. It should be mentioned that the R-centre strain splitting has the opposite sign to I-centre one; the A_{2g} levels here are lower than the E_g ones (see figure 2).

The splitting of the $^5D_1$ and $^7F_1$ manifolds can be caused by two reasons: (1) an electrical field of the electrons located in the CdF_2 layer near Eu^{3+} interface ions, (2) another cation environment; among 12 nearest cation ions of the Eu^{3+} interface ion there are three Cd^{2+} ones. To clarify the main reason for the interface centre appearing, the combined excitation–emission spectra of the $^7F_0 \rightarrow {}^5D_1$ and $^5D_0 \rightarrow {}^7F_1$ transitions in 2, 3 and 5 ML SLs have been measured under additional UV illumination. These measurements are described in [4] and it was concluded that the Eu^{3+} ion electron located near the interface in the CdF_2 layer is the main reason for the optical spectrum transformation. In order to verify this conclusion the calculation of Eu^{3+} energy levels has been carried out.

4. Calculations

The sequence of calculations for impurity centres is as follows: calculation of local crystal structure of impurity centre and then energy levels calculations. For crystal structure calculations we have used the shell model and pair potential approximation. Then the lattice energy can be written as

$$U_{\text{lat}} = \tfrac{1}{2}\sum_i \sum_{k(\neq i)} V_{ik} + \tfrac{1}{2}\sum_i k_i \vec{\delta}_i^2 \tag{1}$$

where $k_i\vec{\delta}_i^2$ is the energy of core–shell interaction of ith ion and V_{ik} is the interaction energy between the ith and kth ions, which can be expressed as

$$V_{ik} = \frac{X_i X_k}{|\vec{r}_i - \vec{r}_k|} + \frac{Y_i X_k}{\left|\vec{r}_i - \vec{r}_k + \vec{\delta}_i\right|} + \frac{X_i Y_k}{\left|\vec{r}_i - \vec{r}_k - \vec{\delta}_k\right|} + \frac{Y_i Y_k}{\left|\vec{r}_i - \vec{r}_k + \vec{\delta}_i - \vec{\delta}_k\right|} + f_{ik}\left(|\vec{r}_i - \vec{r}_k|\right) + g_{ik}\left(\left|\vec{r}_i - \vec{r}_k + \vec{\delta}_i - \vec{\delta}_k\right|\right) \tag{2}$$

where the function

$$f_{ik}(r) = -A_{ik}\exp(-B_{ik}r)/r \tag{3}$$

describes the short-range screening of electrostatic interaction between ion cores, and the function

$$g_{ik}(r) = C_{ik}\exp(-D_{ik}r) - \lambda_{ik}/r^6 \tag{4}$$

Table 2. The short-range interaction potential parameters (atomic units).

Pair	A	B	C	D	λ
F^-–F^-	36.456	1.3778	157.083	1.8927	69.5469
Ca^{2+}–F^-	31.720	1.5490	249.468	2.0421	—
Cd^{2+}–F^-	68.207	1.5453	254.516	2.0574	—
Eu^{3+}–F^-	—	—	196.857	1.9002	—
$k_F = 4.1797$, $k_{Ca} = 11.1692$, $k_{Cd} = 10.6329$, $k_{Eu} = 25.1710$					

Table 3. Lattice constants (Å) of EuF_3 (experiment [11]).

	Experiment	Calculation
a	6.620(1)	6.663
b	7.016(1)	7.586
c	4.392(2)	4.768

Table 4. The position of ions in the EuF_3 cell (experiment [11]).

Atom	Site		x	y	z
Eu	4c	exp.	0.365(1)	0.25	0.063(1)
		calc.	0.371	0.25	0.056
F(1)	4c	exp.	0.522(2)	0.25	0.576(6)
		calc.	0.524	0.25	0.574
F(2)	8f	exp.	0.171(2)	0.065(2)	0.393(4)
		calc.	0.177	0.072	0.406

describes the short-range repulsion between ion shells (which is written in the form of the Born–Mayer potential) and the van der Waals interaction; X_i and Y_i are the core and shell charges of the ith ion, $\vec{r}_i$ is the vector defining the position of the ion core. $\vec{\delta}$ is the vector defining the position of ion shell relative to the ion core. We have used the following values for the core charges: $X_F = +5$, $X_{Ca,Cd} = +8$, $X_{Eu} = +11$. The shell charges have been determined from the condition $Z_i = X_i + Y_i$, where Z_i is the ion charge in the compound. The parameters of the F^-–F^- interaction have been obtained non-empirically by using the Hartree–Fock and the configuration interaction method [9]. The parameters of the Me^{2+}–F^- short-range repulsion and parameter k_i of core–shell interaction for Me^{2+} have been obtained by fitting the calculated crystal properties to the experimental data for the crystals MeF_2 (Me = Ca, Cd): the lattice constants, the dielectric constants ε_0 and ε_∞, the elastic constants C_{11}, C_{12} and C_{44}, the frequencies of the fundamental vibrations ω_{TO} and ω_R. Thus, eight experimental values have been used for fitting three parameters. The parameters of the short-range electrostatic screening have been calculated by numeric integration of the interaction of the free-ion electron densities. The short-range interaction between the metal ions could not be taken into consideration because they are too far from each other. The values of the parameters are given in table 2.

Using these parameters, the lattice constants are 544.7 (CaF_2) and 538.6 (CdF_2) pm. The lattice constants obtained from experiment [10] are 544.3 and 535.6 pm, respectively. The agreement with experiments is very good. The parameters of the Eu–F short-range interaction were fitted to the EuF_3 structure (tables 3 and 4). Three parameters were fitted to twelve experimental values. The agreement with experiments is quite good.

The silicon substrate distorts the CaF_2 and CdF_2 layers. The symmetry is reduced from cubic to rhombohedral. There is a decrease in the angle (from 90° to 89.76°) and also the lattice constant (from 544.3 to 543.5 pm) as a result of this distortion. The values of the distorted angle

and lattice constant were determined from x-ray data. The positions of the ions in the cell are unknown. To take into account the distortion, we fixed the lattice parameters of the fluoride. The ions inside the cell could relax to minimal energy.

For the calculations of the structure of impurity centres, we used the Mott–Littleton method. In the calculations, the internal region around the impurity ion consists of about 1300 ions. And 40 000–85 000 ions, depending on the complication of defects, in the region adjoining the internal region could relax restrictedly. We used the GULP 3.0 program for the calculations.

We calculated the energy levels of Eu^{3+} ($4f^6$) in the remote and interface centres. We used a standard for the lanthanide ion 'effective Hamiltonian' for 4f electrons that acts only within the 4f configuration [12]. The free-ion Hamiltonian parameters were taken from [13]. For the calculations we used programs written by Dr Michael F Reid (University of Canterbury), given to us by the author.

Crystal-field parameters were calculated in the exchange charge model [5]. This takes into account the electrostatic fields generated by point charges and dipoles of the neighbouring ions, as well as the exchange interaction of the 4f shell of the rare-earth ion with ligand electrons. The B_p^q parameters are the sum of the electrostatic and exchange terms:

$$B_p^q = B_{p\,\mathrm{el}}^q + B_{p\,s}^q. \tag{5}$$

The electrostatic term is

$$B_{q\,\mathrm{el}}^p = K_p^q(1-\sigma_p)e^2\left\langle r^p\right\rangle \sum_\alpha (-z_\alpha) P_p^q\,(x_\alpha, y_\alpha, z_\alpha, r_\alpha)\, r_\alpha^{-(2p+1)} \tag{6}$$

where the summation is taken over all the cores and shells of the neighbouring ions having coordinates x_α, y_α, z_α in a fixed Cartesian coordinate system with the centre at the 4f core of the rare-earth ion, r_α is the distance from the lanthanide ion to the core or the shell of the ion of crystal matrix, $P_q^p(x_\alpha, y_\alpha, z_\alpha, r_\alpha)$ are homogeneous polynomials of degree p listed in [14], $\langle r^p\rangle$ is the mean value of r^p for 4f electrons [15], σ_p is the shielding factor which allows for polarization of the closed $5s^25p^6$ shells within the rare-earth ion and its effect on the crystal field at the 4f core, e is the electron charge, Z_α is the effective charge number which takes on the value of X_α for the core and Y_α for the shell of the corresponding ions, and K_q^p are the numerical coefficients arising from the replacement of spherical harmonics by polynomials. Values are given in [5, 16]. The exchange term is

$$B_{q\,s}^p = \frac{2\,(2p+1)}{7} K_p^q e^2 \sum_\alpha S_p\,(r_\alpha)\, P_p^q\,(x_\alpha, y_\alpha, z_\alpha, r_\alpha)\, r_\alpha^{-(p+1)}, \tag{7}$$

where the summation over α is carried out over the cores of the nearest fluorine ions only. Here S_p is the combination of squares of overlap integrals of the 4f wavefunctions of the rare-earth ion with 2s and 2p functions of the fluorine ions:

$$S_p(r) = G_s S_s(r)^2 + G_\sigma S_\sigma(r)^2 + K_p G_\pi S_\pi(r)^2. \tag{8}$$

The dependences of S_s, S_σ, S_π on the rare-earth–F distance can be fitted by the exponential

$$S_k\,(r_\alpha) = S_k^0 \exp\left(-\delta_k r_\alpha^{n_k}\right).$$

The values used were

$$S_s^0 = 0.299, \quad \delta_s = 0.805, \quad n_s = 1.607, \quad S_\sigma^0 = 0.120, \quad \delta_\sigma = 0.431,$$
$$n_\sigma = 1.776, \quad S_\pi^0 = 1.534, \quad \delta_\pi = 2.167, \quad n_\pi = 0.965,$$

where r_α is given in angstroms. These values as well as the shielding constants $\sigma_2 = 0.60$, $\sigma_4 = \sigma_6 = 0$ were calculated and kindly given to us by Professor B Z Malkin. There are three

Table 5. Experimental and calculated energy levels of the cubic centre in bulk CaF_2:Eu^{3+}.

Term	Irreducible representation	Experiment [8] (cm^{-1})	Calculation, this work (cm^{-1})
$^7F_1$	T_{1g}	339	352
$^7F_2$	T_{2g}	812	797
	E_g	1 339	1356
$^7F_3$	T_{1g}	1 855.5	1 882
	T_{2g}	1 968	2 018
	A_{2g}	—	2 210
$^7F_4$	A_{1g}	—	2 398
	T_{1g}	2 884	2 899
	T_{2g}	—	3 178
	E_g	—	3 183
$^7F_5$	T_{2g}	—	3 829
	T_{1g}	—	4 027
	E_g	—	4 255.4
	T_{1g}	—	4 256.0
$^7F_6$	A_{1g}	—	5 047
	T_{1g}	—	5 112
	T_{2g}	—	5 158
	A_{2g}	—	5 351
	T_{2g}	—	5 358
	E_g	—	5 361
$^5D_0$	A_{1g}	17 275.5	17 345
$^5D_1$	T_{1g}	19 030	19 099
$^5D_2$	E_g	21 538	21 524
	T_{2g}	21 428	21 613

Table 6. Crystal-field parameters in cubic and tetragonal centres CaF_2:Eu^{3+} (cm^{-1}).

	Cubic centre		Tetragonal centre	
	Stevens normalization	Wybourne normalization	Stevens normalization	Wybourne normalization
B_0^2	—	—	280	561
B_0^4	−274	−2193	−97	−775
B_4^4	−1370	−1310	−1260	−1205
B_0^6	47	747	61	982
B_4^6	−980	−1397	−688	−981

empirical parameters, G_s, G_σ and G_π, in (8), which are named 'exchange charges'. The parameters are fitted to experimental Stark energy levels. We fitted the parameters to energy levels of cubic centre CaF_2:Eu^{3+} (table 5). Good results were obtained with equal parameters, $G_s = G_\sigma = G_\pi = 9.6$. Thus, only one empirical parameter was used in the model: $G = 9.6$. The crystal-field parameters for the cubic centre CaF_2:Eu^{3+} are shown in table 6.

We calculated the energy levels of the tetragonal centre CaF_2:Eu^{3+} with the same parameter G in order to verify it. Good results have been obtained (see table 7). Crystal-field parameters for the tetragonal centre CaF_2:Eu^{3+} are presented in table 6.

We calculated the energy levels of the remote and interface centres in CdF_2–CaF_2:Eu SLs with the above-mentioned above of parameter G. The calculated values of splitting in $^5D_1$ and $^7F_1$ multiplets for remote centres are 1.1 and 4.7 cm^{-1}. The values determined in experiments

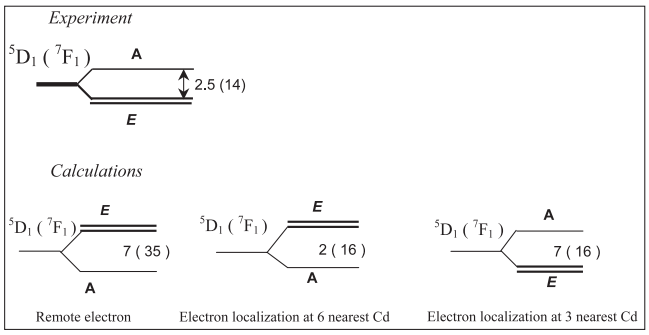

Figure 4. Comparison of the experimental and calculated splitting (using different models) of $^5D_1$ and $^7F_1$ multiplets in the interface centre.

Table 7. Experimental and calculated energy levels of the tetragonal A-centre in bulk CaF_2:Eu^{3+} in (cm^{-1}).

Term	Irrep	Exp. [17] (in air cm^{-1})	Calc., this work
$^7F_1$	E	309	330
	A_2	457	472
$^7F_2$	B_2	852	848
	E	973	971
	B_1	1123	1176
	A_1	1263	1233
$^7F_3$	E	1815	1840
	B_2	1835	1860
	E	1955	1965
	A_2	1976	1986
	B_1	2130	2125
$^7F_4$	A_1	2512	2540
	E	2799	2793
	A_2	2945	2960
	E	3006	3037
	B_1	3089	3049
	B_2	3114	3126
	A_1	3156	3153

are 0.8 and 6.0 cm^{-1}, respectively. It is clear that the calculated values of splitting are in reasonable agreement with the experimental data. The lower level in the $^5D_1$ and $^7F_1$ multiplets is a singlet, in accordance with experimental data. For the $^5D_1$ multiplet we have a discrepancy with experiment: the lower level is a doublet according to our calculations. The discrepancy can be explained by small values of splitting in the $^5D_1$ multiplet.

Three variants of charge compensation have been considered in the interface centre: (i) a charge-compensating electron was removed from the CdF_2/CaF_2 interface, (ii) the electron was localized on the six nearest cadmium ions in the CdF_2 layer, and (iii) the electron was localized on the three nearest cadmium ions in CdF_2. Local crystal structure calculations for the impurity centre were carried out before energy levels calculations in all three cases. We added $-1/6$ (or $-1/3$) to the shell charges of the six (or three) nearest cadmium ions in the crystal structure calculations to take into account the additional electron charge in the last two cases.

It follows from the calculations that in the case when the electron is moved away from CdF_2/CaF_2 interface, the energy structure of $^5D_1$ and $^7F_1$ multiplets is contrary to what the

experimental data suggest: the doublet is higher then the singlet (see figure 4) and the values of A–E splitting are very high. If the charge-compensating electron is localized at the six nearest cadmium ions, the A–E splitting decreases, but the doublet is still higher than the singlet. When the electron is closer and is localized on the three nearest cadmium ions, the doublet is lower than the singlet, as in the experiment. The values of splitting in $^5D_1$ and $^7F_1$ multiplets are also in agreement with experiment.

5. Conclusion

As was demonstrated by the calculations, the splitting of the interface centre Eu^{3+} levels is in good agreement with the experiment with the assumption that the extra charge-compensating electron is localized at three nearest Cd ions. The results confirm the conclusion that the main reason for the optical spectrum transformation of Eu^{3+} in the interface centre is an electron in the neighbouring CdF_2 layer. The calculations showed that the experimentally observed splitting of $^5D_1$ and $^7F_1$ manifolds in the remote centres is caused by the elastic strains existing in the fluoride layers of the pseudomorphic CdF_2–CaF_2 superlattices on silicon.

Acknowledgments

The authors wish to thank Professor B Z Malkin (Kazan State University, Russia) and Dr M F Reid (University of Canterbury, New Zealand) for stimulating discussions. Support from the programmes of the Russian Academy of Sciences ‘New materials and structures’ and the MacDiarmid Institute for Advanced Materials and Nanotechnology (New Zealand) is greatly appreciated.

References

[1] Khilko A Yu, Gastev S V, Kyutt R N, Zamoryanskaya M V and Sokolov N S 1998 *Appl. Surf. Sci.* **123/124** 595–8
[2] Sokolov N S, Gastev S V, Khilko A Yu, Suturin S M, Yassievich I N, Langer J M and Kozanezcki A 1999 *Phys. Rev.* B **59** R2525–8
[3] Gastev S V, Hoffman K R, Choi J K, Krupin A V, Reeves R J and Sokolov N S 2004 *Proc. 12th Int. Symp. Nanostructures: Physics and Technology (St Petersburg)* p 276
[4] Reeves R J, Choi J K, Gastev S V, Krupin A V, Hoffman K R and Sokolov N S 2007 *J. Alloys Compounds* at press
[5] Malkin B Z 1987 *Spectroscopy of Solids Containing Rare-Earth Ions* (Amsterdam: Elsevier Science) p 13
[6] Dieke G H 1968 *Spectra and Energy Levels of Rare Earth Ions in Crystals* ed H M Crosswhite and H Crosswhite (New York: Interscience)
[7] Hamers R J, Wietfeldt J R and Wright J C 1982 *J. Chem. Phys.* **77** 683
[8] Jouart J P, Bouffard M, Klein G and Mary G 1991 *J. Lumin.* **50** 273–7
[9] Nikiforov A E and Shashkin S Yu 1989 *Spectroscopy of Crystals* (Leningrad: Nauka) pp 44–61
[10] Axe J D 1965 *Phys. Rev.* **139** 1215
[11] Zinchenko V F, Efryushina N P, Eryomin O G, Markiv V Ya, Belyavina N M, Mozkova O V and Zakharenko M I 2002 *J. Alloys Compounds* **347** L1
[12] Newman D J and Ng B 2000 *Crystal Field Handbook* (Cambridge: Cambridge University Press) p 290
[13] van Pieterson L, Reid M F, Wegh R T, Soverna S and Meijerink A 2002 *Phys. Rev.* B **65** 045114
[14] Abragam A and Bleaney B 1970 *Electron Paramagnetic Resonance of Transition Ions* (Oxford: Clarendon)
[15] Reid M F, van Pieterson L and Meijerink A 2002 *J. Alloys Compounds* **34** 240
[16] Bumagina L A, Kazakov B N, Malkin B Z and Stolov A L 1977 *Sov. Phys.—Solid State* **19** 624
[17] Wells J-P R 1996 *PhD Thesis* University of Canterbury, NZ (chapter 6)